Phys Chem Minerals (2006) 33:699–709
DOI 10.1007/s00269-006-0116-8

ORIGINAL PAPER

Equation of state of $MgGeO_3$ perovskite to 65 GPa: comparison with the post-perovskite phase

C. E. Runge · A. Kubo · B. Kiefer · Y. Meng · V. B. Prakapenka · G. Shen · R. J. Cava · T. S. Duffy

Received: 17 May 2006 / Accepted: 4 October 2006 / Published online: 26 October 2006

Abstract The equation of state of $MgGeO_3$ perovskite was determined between 25 and 66 GPa using synchrotron X-ray diffraction with the laser-heated diamond anvil cell. The data were fit to a third-order Birch–Murnaghan equation of state and yielded a zero-pressure volume (V_0) of 182.2 ± 0.3 Å^3 and bulk modulus (K_0) of 229 ± 3 GPa, with the pressure derivative ($K'_0 = (\partial K_0/\partial P)_T$) fixed at 3.7. Differential stresses were evaluated using lattice strain theory and found to be typically less than about 1.5 GPa. Theoretical calculations were also carried out using density functional theory from 0 to 205 GPa. The equation of state parameters from theory (V_0 = 180.2 Å^3, K_0 = 221.3 GPa, and K'_0 = 3.90) are in agreement with experiment, although theoretically calculated volumes are systematically lower than experiment. The properties of the perovskite phase were compared to $MgGeO_3$ post-perovskite phase near the observed phase transition pressure (~65 GPa). Across the transition, the density increased by 2.0(0.7)%. This is in excellent agreement with the theoretically determined density change of 1.9%; however both values are larger than those for the $(Mg,Fe)SiO_3$ phase transition. The bulk sound velocity change across the transition is small and is likely to be negative [–0.5(1.6)% from experiment and –1.2% from theory]. These results are similar to previous findings for the $(Mg,Fe)SiO_3$ system. A linearized Birch–Murnaghan equation of state fit to each axis yielded zero-pressure compressibilities of 0.0022, 0.0009, and 0.0016 GPa^{-1} for the *a*, *b*, and *c* axis, respectively. Magnesium germanate appears to be a good analog system for studying the properties of the perovskite and post-perovskite phases in silicates.

Keywords Germanate · Perovskite · Equation-of-state · Lower mantle

C. E. Runge · A. Kubo · T. S. Duffy (✉)
Department of Geosciences, Princeton University, Princeton, NJ 08544, USA
e-mail: duffy@princeton.edu

B. Kiefer
Department of Physics, New Mexico State University, Las Cruces, NM 88003, USA

Y. Meng · G. Shen
HPCAT, Carnegie Institution of Washington, Bldg. 434E, Argonne, IL 60439, USA

V. B. Prakapenka
CARS, University of Chicago, 9700 S Cass Ave., Bldg. 434E, Argonne, IL 60439, USA

R. J. Cava
Department of Chemistry, Princeton University, Princeton, NJ 08544, USA

Introduction

$(Mg,Fe)SiO_3$ perovskite (Pv) is considered to be the dominant phase in the Earth's lower mantle, stable from the 660-km discontinuity to near the core-mantle boundary (Liu 1975, 1976; Knittle and Jeanloz 1987; Fiquet et al. 2000; Shim et al. 2001). At pressure similar to the *D″* discontinuity, $MgSiO_3$ Pv has been observed to undergo a phase transformation to a post-perovskite (pPv) ($CaIrO_3$-type) structure which may be able to explain a number of enigmatic features of the core-mantle boundary region (Murakami et al. 2004).

The equation of state (EOS) of $(Mg,Fe)SiO_3$ Pv has been studied extensively at ambient and high temper-

ature (Knittle and Jeanloz 1987; Horiuchi et al. 1987; Ross and Hazen 1990; Mao et al. 1991; Wang et al. 1994; Fiquet et al. 1998, 2000; Shim and Duffy 2000a; Walter et al. 2004; Vanpeteghem et al. 2006). More recently, the novel phase transformation from $MgSiO_3$ Pv to pPv has spawned numerous experimental and theoretical studies on this high-pressure phase transition (Murakami et al. 2004; Shim et al. 2004; Oganov and Ono 2004; Wookey et al. 2005; Stackhouse et al. 2005; Tsuchiya et al. 2005; Hirose et al. 2006; Wentzcovitch et al. 2006; Shieh et al. 2006; Ono et al. 2006). The phase transition to pPv occurs at very high pressure (~120 GPa), which makes experimental study within its stability field very challenging. Shieh et al. (2006) report an equation of state for $(Mg,Fe)SiO_3$ pPv over 12–106 GPa based on data obtained upon decompression in an Ar pressure medium. Ono et al. (2006) synthesized pPv at 110 GPa and determined the equation of state in the pressure range of 116–144 GPa using a NaCl pressure medium and laser annealing. However, this approach requires long extrapolation to determine the ambient-pressure parameters.

Germanates are widely used as analogs for silicates in high-pressure experiments. $MgGeO_3$ undergoes a similar sequence of phase transitions as $MgSiO_3$ but at lower pressures (Ozima and Akimoto 1983; Ross and Navrotsky 1988; Leinenweber et al. 1994). The first reported synthesis of $MgGeO_3$ in the Pv phase was a transformation from the metastable lithium niobate structure at room temperature and above 12–14 GPa (Leinenweber et al. 1994). Unlike silicate Pv, the germanate Pv reverts to the lithium niobate structure upon decompression. Recently, the phase boundary from the ilmenite phase to Pv phase of $MgGeO_3$ was explored up to 26 GPa and 2,073 K using a large-volume apparatus (Akaogi et al. 2005). The Clapeyron slope of the boundary is negative and can be expressed as P (GPa) = 38.4 – 0.0082 T (K). $FeGeO_3$ has been found to transform to the Pv phase at 33 GPa at room temperature from $FeGeO_3$ clinopyroxene, and it also reverts to the lithium niobate structure upon release of pressure (Nagai et al. 1998; Hattori et al. 1999).

In the germanate system, the Pv–pPv phase transition occurs around 65 GPa (Hirose et al. 2005), compared to about 115–120 GPa in the silicate system (Murakami et al. 2004). $MgGeO_3$ pPv has been synthesized above 60 GPa and its equation of state has been determined up to 200 GPa (Hirose et al. 2005; Kubo et al. 2006). Recently, a study of the deformation behavior of $MgGeO_3$ pPv was carried out using radial X-ray diffraction above 1 Mbar and revealed that slip on (100) or (110) dominates plastic deformation (Merkel et al. 2006).

Although high-pressure studies of $MgGeO_3$ have investigated properties of the pPv phase, no study of the EOS of $MgGeO_3$ Pv phase has been reported. Here we report measurements of the EOS of $MgGeO_3$ Pv and compare properties across the Pv–pPv phases phase transition.

Experimental methods

High-pressure experiments

$MgGeO_3$ orthoenstatite was synthesized as described elsewhere (Kubo et al. 2006). The sample was mixed with 20 wt.% platinum, which served as a pressure calibrant and laser absorber. A symmetric diamond anvil cell (DAC) with 300-μm culets was used for pressure generation. The diamond anvils were backed by tungsten carbide seats with 50° conical openings. The sample was loaded into a 130-μm diameter hole in a Re gasket that had been pre-compressed to ~30-μm thickness. Layers of NaCl sandwiched the sample and acted as both a pressure transmitting medium and as thermal insulation to reduce axial temperature gradients (Kiefer and Duffy 2005).

High-pressure X-ray diffraction experiments were performed at sectors 13-ID-D and 16-ID-B of the Advanced Photon Source, Argonne National Laboratory. In the first run at sector 13-ID-D, 2-D diffraction patterns were collected using either a MAR345 image plate or a MAR-CCD detector. The X-ray beam (λ = 0.3344 Å) was focused to a size of 6 μm × 6 μm using a double mirror system. The distance and orientation of both detectors were calibrated with a CeO_2 standard. The sample was initially compressed to 25 GPa and heated for five minutes above 1,500 K to synthesize the Pv phase. Heating was carried out using a double-sided laser heating system with a TEM_{00} Nd:YLF laser and temperature was measured by spectroradiometry (Shen et al. 2001). The heating spot was ~30 μm in diameter. Pressure was then increased in ~5 GPa intervals to 65 GPa and the sample was heated for approximately 1–3 min above 1,500 K at each pressure step. Diffraction patterns were recorded after heating using 10–30 s exposures for both types of detectors.

The second run was carried out at sector 16-ID-B of the Advanced Photon Source. The doubly focused X-ray (λ = 0.40119 Å) beam size was 10 × 14 μm. A MAR345 image plate was used to collect 2-D diffraction images and was calibrated using a Si standard. The sample was initially compressed to 50 GPa and heated for 5 min at 1,700 K using a single-sided TEM_{01}

Nd:YLF laser to transform the starting material to the Pv phase. The heating spot was ~40 μm in diameter and temperature was measured by spectroradiometry as described above. After heating, diffraction patterns were taken from the center of the heated spot as well as at positions shifted ±10-μm from the heated spot. Detector exposure times ranged between 30 and 100 s. The sample was then decompressed to 30 GPa at pressure steps of ~5 GPa with no further heating. Diffraction patterns were recorded at each step as described above. Peak widths became noticeably broader beginning at pressures below 35 GPa.

2-D images generally showed somewhat spotty $MgGeO_3$ Pv and Pt diffraction rings, with smoother and more continuous NaCl rings consistently throughout both experimental runs. Diffraction patterns at 10 μm from the heated spot showed changes in relative peak intensities and small changes in pressure, but were otherwise similar. The 2-D images were integrated using Fit2D (Hammersley et al. 1996) to obtain corresponding 1-D diffraction patterns. Diffraction peaks were fit to pseudo-Voigt lineshapes after linear background subtraction. Pressure was determined from Pt peak positions using the equation of state of Holmes et al. (1989). For all patterns, Pt diffraction lines 111 and 200 were used, and 220 and 311 were also used when available. In both runs, the difference between pressure calculated by Pt 111 and 200 was 0.5–3.5 GPa, with most pressure differences below 1.5 GPa. Pt peaks 220 and 311 generally yielded pressure values that fell between those of Pt 111 and 200, which is consistent with these pressure differences being due to deviatoric stress.

Computational methodology

First-principle calculations based on Density Functional Theory (Hohenberg and Kohn 1964) were carried out using the same procedure as in our recent study of $MgGeO_3$ pPv (Kubo et al. 2006). The calculations were performed with the software package VASP (Kresse and Hafner 1993, 1994; Kresse and Furthmüller 1996a, b) using the projector-augmented-wave (PAW) method (Blöchl 1994; Kresse and Joubert 1999). Electronic correlations were treated within the local density approximation (LDA) in the parametrization of Perdew and Zunger (1981). We used PAW potentials with core region cut-off radii of 2.0 a.u. for Mg (valence configuration $2p^6 3s^2$), 1.9 a.u. for Ge (valence configuration $3d^{10}4s^2 4p^2$), and 1.52 a.u. for O (valence configuration $2s^2 2p^4$). Tests showed that converged solutions to the Kohn–Sham equations (Kohn and Sham 1965) could be obtained with an energy-cutoff of 600 eV and a $6 \times 4 \times 6$ k-point grid. Total energies are converged to better than 2.3 meV $atom^{-1}$ and stresses due to the incompleteness of the basis-set are less than 0.6 GPa. We optimized the cellshape and all independent internal coordinates for eight volumes between 119 and 180 $Å^3$ in order to determine the groundstate of $MgGeO_3$ at these volumes. The pressure (trace of the stress tensor) and all structural parameters of $MgGeO_3$ Pv were obtained from the relaxed configurations for eight volumes in the pressure range of 0.3 and 205 GPa.

Results

A representative X-ray diffraction pattern at 65 GPa is shown in Fig. 1. $MgGeO_3$ Pv diffraction peaks were indexed to an orthorhombic unit cell (space group *Pbnm*) and at least five peaks were used for cell parameter determination. The cell parameters were computed by least squares fitting using the program Unitcell (Holland and Redfern 1997). The compression data (Fig. 1) were fit using as many peaks from the Pv triplet as possible (020, 112, 200) in addition to the next strongest peaks. Over the entire compression range, these peaks included a subset of 210, 211, 022, 202, 220, 130, 222, 312, and 040. As a result of the laser annealing at each step in this run, there was more variability in observed peak intensities due to texturing. These intensity variations and some peak overlaps prevented us from using the same set of peaks at each pressure in this experiment. For the decompression run, Pv peaks 020, 112, 200, 202, and 122 were used consistently for each pressure.

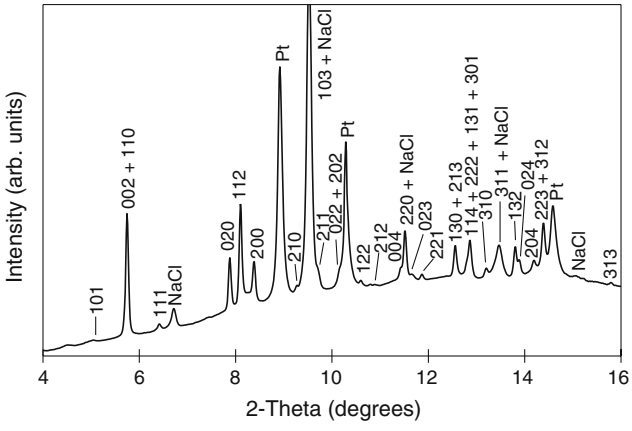

Fig. 1 Representative X-ray diffraction pattern at 65 GPa during the compression run. $MgGeO_3$ Pv peaks are labeled with their respective *hkl*. Also indicated are peaks from NaCl (B2 phase) and Pt

Pressure–volume data from both experiment and theory were fitted using a third order Birch–Murnaghan equation of state:

$$P = \frac{3}{2}K_0\left[\left(\frac{V_0}{V}\right)^{\frac{7}{3}} - \left(\frac{V_0}{V}\right)^{\frac{5}{3}}\right] \times \left\{1 - \frac{3}{4}(4 - K_0^{'}) \times \left[\left(\frac{V_0}{V}\right)^{\frac{2}{3}} - 1\right]\right\}, \quad (1)$$

where V_0, K_0, and K'_0, are the zero-pressure volume, isothermal bulk modulus, and pressure derivative of the isothermal bulk modulus, respectively. Pressure–volume data for both experimental runs are shown in Fig. 2 and Table 1. All data were recorded within (or very near to) the stability field of Pv in a pressure range between 24 and 66 GPa. Our pressure–volume data are also in good agreement with a single datum at 17.9 GPa reported by Leinenweber et al. (1994).

Due to the difficulty of simultaneously constraining K_0, V_0, and K'_0 from static compression data (Bass et al. 1981), we used an additional constraint from elasticity systematics following a recent study on $MgGeO_3$ pPv (Kubo et al. 2006). The semi-empirical relation $K_0 \cdot V_0$ = constant has been shown to hold for many isostructural materials (Anderson and Anderson 1970; Liebermann et al. 1977). Experimental and theoretical studies yield $K_0 \cdot V_0 = 63$ cm^3 Mbar mol^{-1} for $MgSiO_3$ Pv (e.g., Fiquet et al. 1998, 2000; Oganov and Ono 2004; Vanpeteghem et al. 2006). We fixed K'_0 for $MgGeO_3$ Pv at the value which results in K_0 and V_0 values that match the relationship from systematics. Our fitting procedure resulted in a fixed K'_0 of 3.7, $K_0 = 229 \pm 3$ GPa, and $V_0 = 182.2 \pm 0.3$ Å^3 for $MgGeO_3$ Pv. For comparison, when K'_0 is fixed at 4.0, we obtain a K_0 of 216 ± 3 GPa and V_0 of 182.9 ± 0.3 Å^3. When K'_0 is lowered, K_0 increases faster then V_0 decreases, ultimately producing larger values of $K_0 \cdot V_0$. To illustrate the effects of pressure determination on the EOS, if pressure values are calculated solely from the Pt 111 reflection, fit parameters change minimally with a slight increase in K_0 of ~5 GPa and no change in zero-pressure volume.

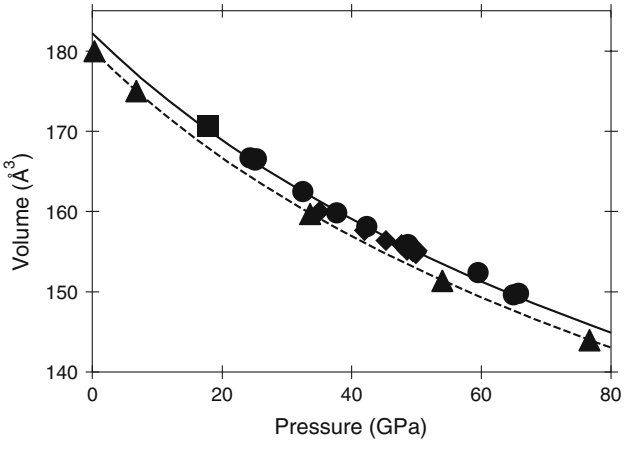

Fig. 2 Pressure–volume data for $MgGeO_3$ Pv phase. *Solid curve* is a fit using third order Birch–Murnaghan EOS. *Dashed line* is a third order Birch–Murnaghan EOS fit to the theoretical data. *Solid circles and diamonds* experimental compression and decompression data, respectively; *solid triangles* theoretical calculations; *solid square* Leinenweber et al. (1994)

An EOS fit to the pressure–volume data obtained from the first principles calculations for $MgGeO_3$ Pv yielded $K_0 = 221.3 \pm 0.7$ GPa, $V_0 = 180.16 \pm 0.05$ Å^3, and $K'_0 = 3.90 \pm 0.01$ (Fig. 2, Table 2), in good agreement with our experimental EOS. The theoretically calculated volumes are systematically lower than the experimental volumes, which is typical of LDA calculations. This was also observed in our previous study of $MgGeO_3$ pPv (Table 3) (Kubo et al. 2006). The discrepancy is also attributed in part to the 300 K temperature difference between experiment and theory. A systematic shift of +5 GPa to the theoretical data points would be required to bring the calculated and measured equations of state into agreement (cf. Oganov et al. 2001).

Discussion

Equation of state

Figure 3 compares experimental pressure–volume data for both the Pv and pPv phases of magnesium germanate. As expected, the volumes of Pv are larger than pPv. For pPv, lower pressure data below the Pv–pPv transition pressure exhibit peak broadening and anomalously large volumes so only data above 47 GPa were used in the fitting (Kubo et al. 2006). At 65 GPa, we find the germanate pPv phase is 2.0(0.7)% denser than the Pv phase (Table 4). This is in excellent agreement with an increase of 1.9% predicted by our first-principles calculations. This density increase is larger than the 1.1–1.6 % density change observed or calculated for the transformation in the $(Mg,Fe)SiO_3$ system (Oganov and Ono 2004; Tsuchiya et al. 2005; Shieh et al. 2006).

The ambient-pressure bulk modulus and pressure derivative were converted from isothermal to adiabatic values for the Pv and pPv phase using thermodynamic relations (Speziale and Duffy 2002) and either measured or estimated values for the relevant parameters

Table 1 Refined cell parameters and volume of $MgGeO_3$ Pv

Pressure (GPa)	*a* (Å)	*b* (Å)	*c* (Å)	Volume (Å^3)
25.1 (6) c	4.7857 (22)	4.9938 (22)	6.9638 (14)	166.43 (32)
25.3 (5) c	4.7861 (14)	4.9927 (14)	6.9706 (8)	166.57 (20)
24.3 (5) c	4.7848 (8)	4.9989 (8)	6.9694 (37)	166.70 (7)
32.4 (8) c	4.7363 (10)	4.9653 (11)	6.9090 (37)	162.48 (7)
35.0 (10) d	4.6990 (10)	4.9587 (61)	6.8683 (29)	160.04 (6)
37.7 (13) c	4.7096 (16)	4.9441 (17)	6.8642 (52)	159.83 (10)
42.0 (8) d	4.6743 (16)	4.9390 (10)	6.8285 (50)	157.65 (10)
42.3 (21) c	4.6970 (28)	4.9280 (27)	6.8323 (91)	158.15 (20)
45.2 (5) d	4.6586 (20)	4.9260 (18)	6.8154 (59)	156.40 (12)
47.7 (4) d	4.6510 (35)	4.9121 (20)	6.8223 (10)	155.86 (21)
48.4 (8) d	4.6486 (43)	4.9109 (36)	6.8190 (13)	155.67 (26)
48.5 (9) d	4.6483 (28)	4.9100 (13)	6.7993 (82)	155.18 (17)
48.6 (6) d	4.6470 (44)	4.9090 (43)	6.824 (13)	155.68 (26)
48.7 (13) c	4.6583 (42)	4.9101 (15)	6.8162 (56)	155.91 (10)
49.4 (8) d	4.6430 (16)	4.9063 (34)	6.8032 (47)	154.98 (10)
49.6 (7) d	4.6430 (34)	4.9049 (16)	6.813 (10)	155.16 (21)
49.9 (8) d	4.6426 (13)	4.9042 (20)	6.7987 (37)	154.79 (8)
49.9 (7) d	4.6463 (20)	4.9048 (35)	6.7947 (58)	154.85 (12)
49.9 (8) d	4.6428 (13)	4.9061 (45)	6.8008 (37)	154.91 (7)
50.1 (14) d	4.6453 (33)	4.9054 (28)	6.8080 (99)	155.13 (2)
59.5 (18) c	4.6331 (15)	4.8724 (26)	6.751 (16)	152.41 (26)
64.9 (1) c	4.5754 (8)	4.8676 (8)	6.7194 (24)	149.65 (5)
65.7 (16) c	4.5869 (10)	4.8603 (10)	6.7208 (32)	149.83 (7)

Numbers in parentheses are one standard deviation uncertainties
c Compression, *d* decompression

(Shim and Duffy 2000a; Li and Zhang 2005). We obtain K_{S0} = 231.3 GPa and K'_{S0} = 3.67 from our experimental data. The adiabatic bulk modulus was then computed as a function of pressure by using third-order Eulerian finite strain expressions (Davies and Dziewonski 1975). At 65 GPa, the adiabatic bulk moduli were almost identical for the two phases at this pressure: K_S = 456(7) GPa for Pv and K_S = 461(13) GPa for pPv (Table 4). From theoretical calculations, the bulk moduli of the Pv and pPv phases at the same pressures are 455 and 452 GPa, respectively. Thus, both theory and experiment consistently indicate that the change in bulk modulus across the transition is small, and is less than the uncertainties.

Table 2 Cell parameters and volume of $MgGeO_3$ Pv at 0 K from theoretical calculations

Pressure (GPa)	*a* (Å)	*b* (Å)	*c* (Å)	Volume (Å^3)
0.3	4.915	5.100	7.181	180.00
6.8	4.864	5.063	7.106	175.00
33.6	4.692	4.951	6.874	159.70
54.0	4.588	4.891	6.745	151.38
76.7	4.490	4.839	6.628	144.00
95.5	4.417	4.805	6.546	138.91
118.2	4.337	4.770	6.460	133.66
205.6	4.097	4.674	6.214	119.00

The bulk sound velocity, V_B, of each phase at 65 GPa was calculated (Table 4) from the density and adiabatic bulk modulus using the relation: $V_B = \sqrt{K_S/\rho}$. The change in V_B across the transition as determined from experiment [–0.5(1.6)%] and theory (–1.2%) are also both small. Both experiment and theory suggest a negative change in V_B across the transition, but experimental uncertainties allow for small positive changes as well. This is consistent with both theoretical and experimental data for the $(Mg,Fe)SiO_3$ system which also indicate a small and likely negative change in bulk sound velocity across the transition (Oganov and Ono 2004; Iitaka et al. 2004; Shieh et al. 2006).

Table 3 Equation of state parameters

Formula	Phase	V_0 (Å^3)	K_0 (GPa)	K'_0	Method
$MgGeO_3$	Pv	182.2 (0.3)	229 (3)	3.7[i]	Exp[a, j]
$MgGeO_3$	Pv	182.9 (0.3)	216 (3)	4.0[i]	Exp[a]
$MgGeO_3$	Pv	180.16 (5)	221.3 (7)	3.90 (1)	Theory[a]
$MgGeO_3$	pPv	179.2 (7)	207 (5)	4.4[i]	Exp[b]
$MgGeO_3$	pPv	178.0	201.9	4.3	Theory[b]
$MgSiO_3$	Pv	162.3[i]	260 (9)	3.7 (4)	Exp[c]
$MgSiO_3$	Pv	162.6 (2)	253 (1)	4.0[i]	Exp[d]
$MgSiO_3$	Pv	163.4	259.8	4.1	Theory[e]
$MgSiO_3$	pPv	162.9	231.9	4.4	Theory[e]
$MgSiO_3$	pPv	163.8	215.9	4.4	Theory[f]
$MgSiO_3$	pPv	162.86[i]	237 (1)	4.0[i]	Exp[g]
$(Mg,Fe)SiO_3$	pPv	164.9 (6)	219 (5)	4.0[i]	Exp[h]

[a] This study, [b]Kubo et al. (2006), [c]Fiquet et al. (2000), [d]Vanpeteghem et al. (2006), [e]Oganov and Ono (2004), [f]Tsuchiya et al. (2005), [g]Ono et al. (2006), [h]Shieh et al. (2006), [i]Fixed value, [j]Best fit with elasticity systematics

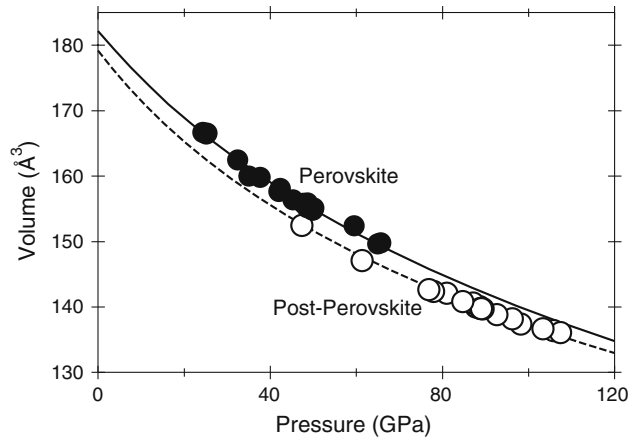

Fig. 3 Comparison of experimental pressure–volume measurements for $MgGeO_3$ Pv and pPv phases. *Solid circles* Pv data (this study); *open circles* pPv data (Kubo et al. 2006). *Solid and dashed curves* are fits using third order Birch–Murnaghan EOS for the Pv and pPv studies, respectively. Data below 47 GPa for the pPv phase were not used in the equation of state determination and are not shown (Kubo et al. 2006)

Table 4 $MgGeO_3$ properties at 65 GPa

	ρ (g cm^{-3})	K_S (GPa)	V_B(km s^{-1})
Experiment			
Pv	6.43 (2)	456 (7)	8.42 (6)
pPv	6.56 (4)	461 (13)	8.38 (12)
Theory			
Pv	6.52	455	8.35
pPv	6.65	452	8.24

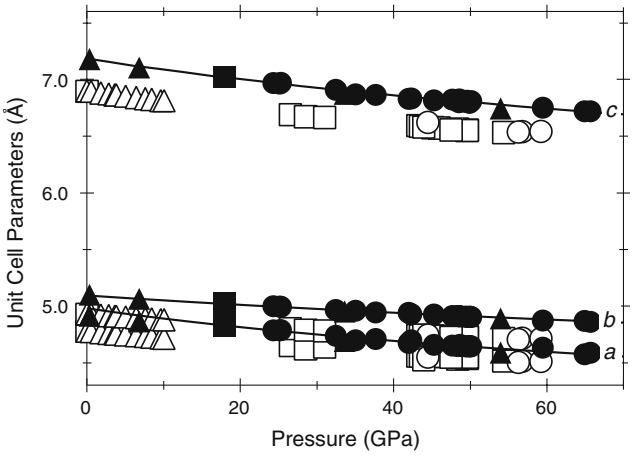

Fig. 4 Axial lengths for $MgGeO_3$ and $MgSiO_3$ Pv phase. *Solid circles and triangles* represent $MgGeO_3$ experimental and theoretical results for this study, respectively. *Solid lines* correspond to the best fit of each axis to the modified Birch–Murnaghan equation. Datum of Leinenweber et al. (1994) is represented by *solid square*. *Open symbols* are data points for $MgSiO_3$ Pv. *Squares, circles, and triangles* are from Fiquet et al. (1998, 2000), Walter et al. (2004), and Vanpeteghem et al. (2006), respectively

Lattice parameters

Figure 4 shows cell parameters of germanate and silicate Pv versus pressure. For the germanate, the cell axes exhibit similar trends as silicates but are systematically larger due to the larger ionic radius of Ge^{4+} as compared to Si^{4+}. The present results also agree well with the datum for $MgGeO_3$ Pv reported at 17.9 GPa by Leinenweber et al. (1994). Theoretical values fall slightly below experiment. Further comparison of theory and experiment is provided by axial ratios plotted in Fig. 5. Experiment and theory are in good agreement, and show that both c/a and b/a increase with compression.

Unit cell parameters were fit using a form of the third-order finite strain (Birch–Murnaghan) equation modified for axial compression (Meade and Jeanloz 1990; Xia et al. 1998; Angel 2000):

$$P = \frac{3}{2}K_{l0}\left[\left(\frac{l_0}{l}\right)^7 - \left(\frac{l_0}{l}\right)^5\right] \times \left\{1 - \frac{3}{4}\left(4 - K'_{l0}\right) \times \left[\left(\frac{l_0}{l}\right)^2 - 1\right]\right\}, \quad (2)$$

where K_{l0}, and K_{l0}' are the zero-pressure incompressibility and pressure derivative of the l-axis ($l = a, b, c$). From fits to the experimental data, the values of a_0, b_0, and c_0 obtained at ambient P were 4.981(40), 5.093(19), and 7.184(42) Å, respectively, which agree with theory within about 1.3% or better. The relative axial compressibilities for germanate and silicate Pv are shown in Fig. 6. The zero-pressure axial compressibility, β_l, was determined from Eq. 2 using the relation (Xia et al. 1998):

$$\beta_l = -\frac{1}{l}\left(\frac{\partial l}{\partial P}\right)_T = \frac{1}{(3K_l)}. \quad (3)$$

Zero-pressure compressibilities from the germanate Pv experimental data were found to be 0.0022, 0.0009, 0.0016 GPa^{-1} for the a, b, and c-axis, respectively, with K_{l0}' fixed at 4.0 for all axes (Fig. 6a). Zero-pressure compressibilities obtained from fitting theoretical data to 77 GPa and using a fixed K_{l0}' of 4.0 are: 0.0020, 0.0010, and 0.0017 GPa^{-1}, in good agreement with experiment. A fourth-order term may be required to fit the theoretical b-axis data at higher pressures.

Both theory and experiment are consistent in finding that the b-axis is the least compressible axis, the a-axis is the most compressible, and the c-axis is intermediate. $MgSiO_3$ Pv shows the same order of compressibility for

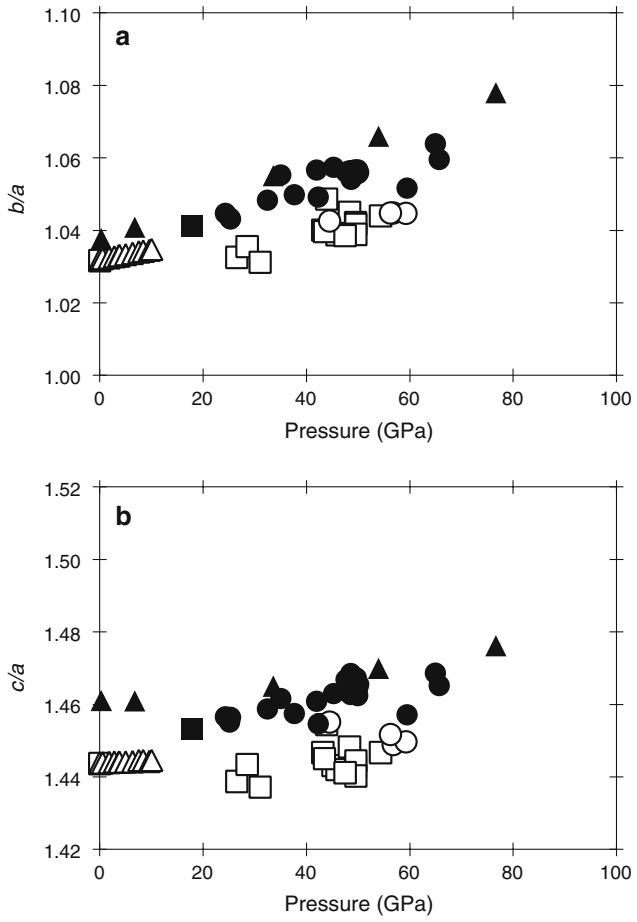

Fig. 5 Axial ratios for **a** *b/a*, and **b** *c/a* for $MgGeO_3$ and $MgSiO_3$ Pv. Symbols are the same as in Fig. 4

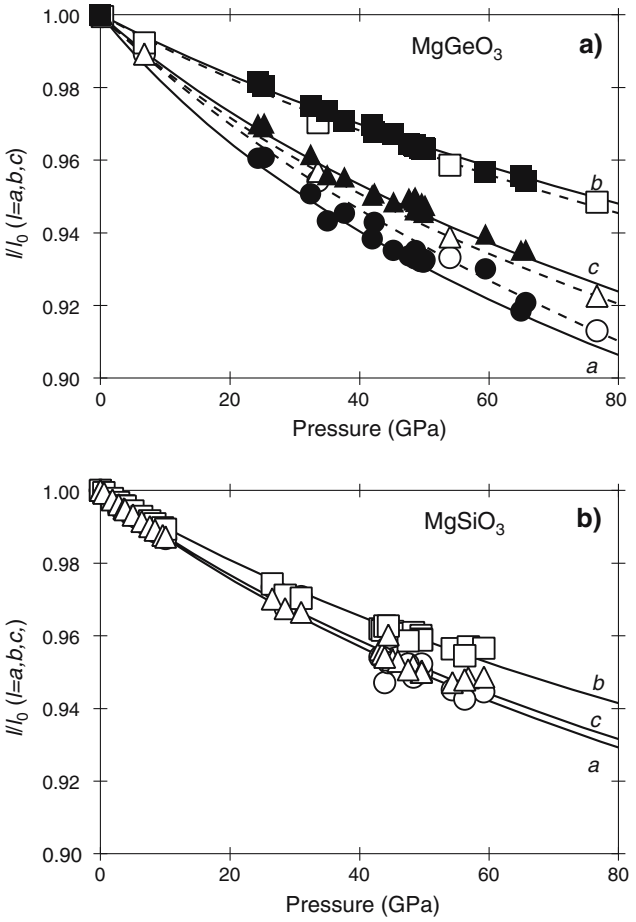

Fig. 6 Linear compressibilities of the unit cell axes for $MgGeO_3$ and $MgSiO_3$ Pv. *Circles, squares, and triangles* represent *a, b*, and *c*-axis, respectively; **a** *solid symbols and lines* represent $MgGeO_3$ Pv experimental data points and modified Birch–Murnaghan fit. *Open symbols and dashed line* represent $MgGeO_3$ Pv theory data points and fit; and **b** combined compressibility dataset of $MgSiO_3$. Previous studies of Fiquet et al. (1998, 2000), Walter et al. (2004), and Vanpeteghem et al. (2006) are represented by *open symbols*, and solid best fit line is from modified Birch–Murnaghan equation

the three axes (Fig. 6b). However the *a*- and *c*-axes of the silicate exhibit more similar compressibility than for the germanate. Combining data sets from previous $MgSiO_3$ Pv studies (Fiquet et al. 1998, 2000; Walter et al. 2004; Vanpeteghem et al. 2006) the zero-pressure incompressibilities were determined using the same fitting procedure as described for experimental data above. The compressibility of the axes for the silicate were found to be 0.0014, 0.0011, and 0.0014 GPa^{-1} and in agreement with results reported by other studies (e.g., Vanpeteghem et al. 2006).

Stress state

Deviatoric stresses in the samples were evaluated for both compression and decompression runs using diffraction peaks from the Pt pressure standard. Differential stress in the DAC due to uniaxial compression can be described using lattice strain theory (Singh 1993). The presence of deviatoric stress results in small differences in lattice parameters computed from individual diffraction lines of a cubic material. The difference in lattice parameter of the 111 and 200 lines under differential stress in an axial angle-dispersive geometry can be written as

$$\frac{a_{(111)} - a_{(200)}}{a_0} = -\frac{St}{3}\left[1 - 3\cos^2(90^\circ - \theta_{111})\right] - \frac{(S_{11} - S_{12})t}{3}\left[(1 - 3\cos^2(90^\circ - \theta_{111})) - (1 - 3\cos^2(90^\circ - \theta_{200}))\right], \quad (4)$$

where a_0 is the zero-pressure lattice parameter, $t = \sigma_3 - \sigma_1$ is the differential stress in which σ_1 is the stress along the radial direction of the DAC and σ_3 the stress along the axial direction. θ_{hkl} refers to the

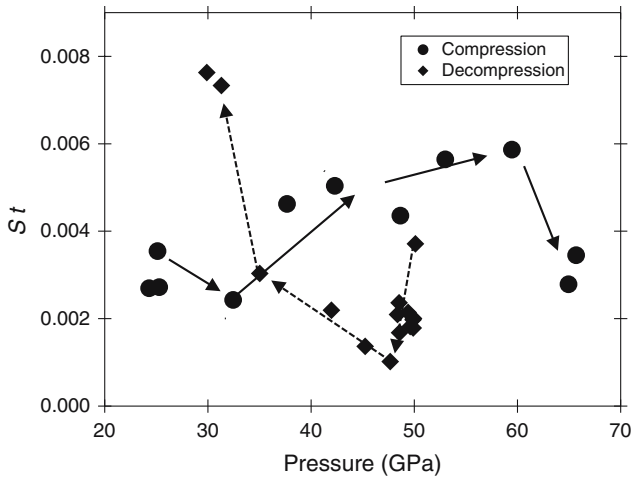

Fig. 7 Calculated *St* values based on 111 and 200 reflections for platinum. *Solid circles* compression, *solid diamonds* decompression. *Solid and dashed lines* are guides to the eye

diffraction angle for a given *hkl* value. *S*, the elastic anisotropy, is given by

$$S = S_{11} - S_{12} - \frac{S_{44}}{2}, \tag{5}$$

where S_{ij} correspond to single-crystal elastic compliances.

The θ values for Pt 111 or 200 are approximately 4.3° and 5.0°, respectively, for the compression run, and 5.3° and 6.1° for the decompression run. Due to the similarity of the θ values, the second term on the right hand side of Eq. 4 is small compared with the first term and can be neglected. We can thus use a simplified expression to quantify differential stress in the experiments (Shim et al. 2000b):

$$\frac{a_{(111)} - a_{(200)}}{a_0} = -\frac{St}{3}\left[1 - 3\cos^2(90 - \theta_{111})\right]. \tag{6}$$

S has been determined for Pt only at ambient conditions from single-crystal elasticity measurements (MacFarlane et al. 1965) but the effect of pressure on anisotropy is inferred to be small from radial X-ray diffraction measurements (Kavner and Duffy 2003). Therefore, we use parameter *St* to characterize the stress state in the DAC for each data point, and assume that *S* does not change with pressure.

Figure 7 shows *St* values versus pressure for compression and decompression experimental runs. For the decompression run down to ~35 GPa, *St* values range between 0.0010 and 0.0037. Using the ambient-pressure value $S = 0.0039$ GPa^{-1} (MacFarlane et al. 1965), this corresponds to differential stresses of 0.3–1.0 GPa. For the compression run, *St* ranges from 0.0024 to 0.0059 corresponding to differential stresses of 0.6–1.5 GPa. For comparison, measurements of differential stress in Pt using the radial diffraction method yield values of 2.5–3.3 GPa at 5–22 GPa confining pressure (Kavner and Duffy 2003). Assuming these correspond to the yield strength and extrapolating linearly to the pressure range of the present experiments (25–66 GPa), it is expected that the maximum supported differential stresses in Pt is 3.4–5.3 GPa. Thus, while differential stresses up to 1.5 GPa are estimated in the present experiments, the observed differential stresses are well below the maximum stress (yield strength) that Pt can support under these conditions. The strength of $MgGeO_3$ Pv is unknown but is expected to be much larger than that of Pt based on available data for silicates and germanates (Shieh et al. 2004; Merkel et al. 2006). Therefore, the differential stresses observed in Pt are likely to be representative of the *t* values existing in Pv as well.

Figure 7 shows that our laser annealing was only partially successful in reducing differential stresses, consistent with observations from other laser heating experiments using NaCl pressure media (Kavner and Duffy 2001). In general, during compression, the differential stress increased with increasing pressure even after laser annealing. In the decompression run, the situation was different. The apparent differential stress at first decreased upon decompression and reached a minimum value at 47 GPa. Subsequently the differential stress began to increase again. Below 35 GPa significant peak broadening was observed which corresponded to a sharp increase of the *St* values. Consequently, two data points below this pressure were not used in the fitting of the equation of state. These results suggest that there are strong variations in differential stress during the decompression process, and that the evolution of differential stresses during compression and decompression may be different. In our companion study of $MgGeO_3$ pPv (Kubo et al. 2006), the inferred differential stresses in Pt were 0–2 GPa from 45–184 GPa compared with extrapolated yield strengths for Pt of 4.5–10.9 GPa. Thus, the overall differential stress levels are similar in both experiments. Notably, during decompression experiments on $MgGeO_3$ pPv, Kubo et al. (2006) also observed a similar trend whereby the differential stress at first decreased with decompression but then increased rapidly after a certain pressure and was accompanied by a distinct broadening of the diffraction peaks as well as anomalously large measured volumes.

Conclusion

Experimental and theoretical equations of state for $MgGeO_3$ Pv are in excellent agreement. Experimental values of K_0 and V_0 were constrained to be 229 ± 3 GPa and 182.2 ± 0.3 Å^3, respectively, with a fixed K'_0 of 3.7. Theoretical calculations yield similar values of V_0 = 180.2 Å^3, K_0 = 221.3 GPa, and K'_0 = 3.90. Using these results together with $MgGeO_3$ pPv data obtained by Kubo et al. (2006), changes across the Pv–pPv phase transition were quantified from direct comparison between the two phases. Observed changes in density of 2.0(0.7)% and bulk sound speed of –0.5(1.6)% for the $MgGeO_3$ system compare favorably with the theoretical values of an 1.9% increase in density and a change in bulk sound speed of –1.2%. These results are comparable to those observed or calculated in the $MgSiO_3$ system.

$MgGeO_3$ Pv axial lengths and their ratios were also in agreement between theory and experiment. Zero-pressure compressibilities of the germanate were determined to be 0.0022, 0.0009, 0.0016 GPa^{-1} for the *a, b*, and *c* axis, respectively. This is in excellent agreement with the zero-pressure compressibilities of 0.0020, 0.0010, 0.0017 GPa^{-1} found theoretically. The germanate and silicate Pv also show similar axial trends, and exhibit the same order of compressibility of the three axes, although the *a* and *c*-axes of the germanate show more anisotropy than in the silicate. In contrast, germanate post-perovskite shows less anisotropy in compressibility than silicate post-perovskite (Kubo et al. 2006).

These results have implications for understanding the pPv phase transformation in the Earth's mantle. Because of the extreme pressure at which the Pv–pPv phase transition occurs, theoretical studies on silicates (e.g., Oganov and Ono 2004; Tsuchiya et al. 2005; Wentzcovitch et al. 2006) and experiments on germanates (Hirose et al. 2005; Merkel et al. 2006; Kubo et al. 2006) have played a prominent role in establishing the physical and mechanical properties of the high-pressure phase. Our study, together with earlier work (Kubo et al. 2006), demonstrates that theory and experiment yield consistent results for equation of state parameters and axial compressibilities in an analog system (albeit with a systematic shift in lattice parameters and volumes). This provides support for the reliability of theoretical calculations of the magnesium silicate pPv phase.

The change in density and sound velocity across phase transitions are fundamental parameters for assessing whether the phase transformation is consistent with seismic data. Our results show that changes in physical properties (density, bulk modulus, and bulk sound velocity) across the Pv–pPv transition are similar in germanates and silicates. In particular, we find a small change in the bulk modulus and a likely decrease in the bulk sound velocity across the transition consistent with results on the silicate transformation (Oganov and Ono 2004; Tsuchiya et al. 2005; Shieh et al. 2006). This may provide an explanation for seismic features of *D″* such as the stronger discontinuity observed for shear waves than compressed waves (e.g., Wookey et al. 2005).

Deformation studies on $MgGeO_3$ pPv have been used to infer slip systems relevant to understanding deformation and seismic anisotropy in the deep mantle (Merkel et al. 2006). Our results provide general support for the concept that germanates may be suitable analogs for the mechanical behavior of silicates at high pressures, although there are some differences in the structural anisotropy of germanate and silicate perovskites.

Acknowledgments Henry Scott (IUSB) provided experimental assistance. We also thank the staffs of GSECARS and HPCAT. This work was performed at GeoSoilEnviroCARS (Sector 13) and HPCAT (Sector 16), Advanced Photon Source (APS), Argonne National Laboratory. GeoSoilEnviroCARS is supported by the NSF, DOE, and the State of Illinois. Use of the HPCAT facility was supported by DOE-BES, DOE-NNSA (CDAC), NSF, DOD-TACOM, and the W.M. Keck Foundation. Use of the APS was supported by the U.S. Department of Energy, Office of Basic Energy Sciences.

References

Akaogi M, Kojitani H, Yusa H, Yamamoto R, Kido M, Koyama K (2005) High-pressure transitions and thermochemistry of $MGeO_3$ (M = Mg, Zn and Sr) and Sr-silicates: systematics in enthalpies of formation of $A^{2+}B^{4+}O_3$ perovskites. Phys Chem Miner 32:603–613

Anderson DL, Anderson OL (1970) Bulk modulus–volume relationship for oxides. J Geophys Res 75:3494–3500

Angel RJ (2000) Equations of state. Rev Miner Geochem 41:35–59

Bass JD, Liebermann RC, Weidner DJ, Finch SJ (1981) Elastic properties from acoustic and volume compression experiments. Phys Earth Planet Inter 25:140–158

Blöchl PE (1994) Projector augmented-wave method. Phys Rev B 50:17953–17979

Davies GF, Dziewonski AM (1975) Homogeneity and constitution of the earth's lower mantle and outer core. Phys Earth Planet Inter 10:336–343

Fiquet G, Andrault D, Dewaele A, Charpin T, Kunz M, Haüsermann D (1998) *P–V–T* equation of state of $MgSiO_3$ perovskite. Phys Earth Planet Inter 105:21–31

Fiquet G, Dewaele A, Andrault D, Kunz M, LeBihan T (2000) Thermoelastic properties and crystal structure of $MgSiO_3$ perovskite at lower mantle pressure and temperature conditions. Geophys Res Lett 27:21–24

Hammersley AP, Svensson SO, Hanfland M, Fitch AN, Haüsermann D (1996) Two-dimensional detector software: from

real detector to idealized image or two-theta scan. High Press Res 14:235–248
Hattori T, Matsuda T, Tsuchiya T, Nagai T, Yamanaka T (1999) Clinopyroxene–perovskite phase transition of $FeGeO_3$ under high pressure and room temperature. Phys Chem Miner 26:212–216
Hirose K, Kawamura K, Ohishi Y, Tateno S, Sata N (2005) Stability and equation of state of $MgGeO_3$ post-perovskite phase. Am Mineral 90:262–265
Hirose K, Karato S, Cormier VF, Brodholt JP, Yuen DA (2006) Unsolved problems in the lowermost mantle. Geophys Res Lett 33:L12S01
Hohenberg P, Kohn W (1964) Inhomogeneous electron gas. Phys Rev B 136:864–871
Holland TJB, Redfern SAT (1997) UnitCell: a nonlinear least-squares program for cell-parameter refinement implementing regression and deletion diagnostics. J Appl Crystallogr 30:84
Holmes NC, Moriarty JA, Gathers GR, Nellis WJ (1989) The equation of state of platinum to 660 GPa (6.6 Mbar). J Appl Phys 66:2962–2967
Horiuchi H, Ito E, Weidner DJ (1987) Perovskite-type $MgSiO_3$: single-crystal X-ray diffraction study. Am Mineral 72:357–360
Iitaka T, Hirose K, Kawamura K, Murakami M (2004) The elasticity of the $MgSiO_3$ post-perovskite phase in the Earth's lowermost mantle. Nature 430:442–445
Kavner A, Duffy TS (2001) Pressure–volume–temperature paths in the laser-heated diamond cell. J Appl Phys 89:1907–1914
Kavner A, Duffy TS (2003) Elasticity and rheology of platinum under high pressure and nonhydrostatic stress. Phys Rev B 68:144101
Kiefer B, Duffy TS (2005) Finite element simulations of the laser-heated diamond-anvil cell. J Appl Phys 97:114902
Knittle E, Jeanloz R (1987) Synthesis and equation of state of (Mg, Fe)SiO_3 perovskite to over 100 gigapascals. Science 235:668–670
Kohn W, Sham LJ (1965) Self-consistent equations including exchange and correlation effects. Phys Rev 140:1133–1138
Kresse G, Furthmüller J (1996a) Efficiency of ab-initio total energy calculations for metals and semiconductors using a plane-wave basis set. Comput Mat Sci 6:15–50
Kresse G, Furthmüller J (1996b) Efficient iterative schemes for ab initio total-energy calculations using a plane-wave basis set. Phys Rev B 54:11169–11186
Kresse G, Hafner J (1993) Ab initio molecular dynamics for liquid metals. Phys Rev B 47:558–561
Kresse G, Hafner J (1994) Ab initio molecular-dynamics simulation of the liquid-metal–amorphous-semiconductor transition in germanium. Phys Rev B 49:14251–14269
Kresse G, Joubert D (1999) From ultrasoft pseudopotentials to the projector augmented-wave method. Phys Rev B 59:1758–1775
Kubo A, Kiefer B, Shen G, Prakapenka VB, Cava RJ, Duffy TS (2006), Stability and equation of state of the post-perovskite phase in $MgGeO_3$ to 2 Mbar. Geophys Res Lett 33:L12S12
Leinenweber K, Wang Y, Yagi T, Yusa H (1994) An unquenchable perovskite phase of $MgGeO_3$ and comparison with $MgSiO_3$ perovskite. Am Mineral 79:197–199
Li B, Zhang J (2005) Pressure and temperature dependence of elastic wave velocity of $MgSiO_3$ perovskite and the composition of the lower mantle. Phys Earth Planet Inter 151:143–154
Liebermann RC, Jones LEA, Ringwood AE (1977) Elasticity of aluminate, titanate, stannate and germanate compounds with the perovskite structure. Phys Earth Planet Inter 14:165–178
Liu LG (1975) Post-oxide phases of olivine and pyroxene and mineralogy of the mantle. Nature 258:510–512
Liu LG (1976) Orthorhombic perovskite phases observed in olivine, pyroxene and garnet at high-pressures and temperatures. Phys Earth Planet Inter 11:289–298
MacFarlane RE, Rayne JA, Jones CK (1965) Anomalous temperature dependence of shear modulus c_{44} for platinum. Phys Lett 18:91–92
Mao H-K, Hemley RJ, Fei Y, Shu JF, Chen LC, Jephcoat AP, Wu Y, Bassett WA (1991) Effect of pressure, temperature, and composition on lattice parameters and density of (Fe,Mg)SiO_3-perovskites to 30 GPa. J Geophys Res 96:8069–8079
Meade C, Jeanloz R (1990) Static compression of $Ca(OH)_2$ at room-temperature—observations of amorphization and equation of state measurements to 10.7 GPa. Geophys Res Lett 17:1157–1160
Merkel S, Kubo A, Miyagi L, Speziale S, Duffy TS, Mao H-K, Wenk H-R (2006) Plastic deformation of $MgGeO_3$ post-perovskite at lower mantle pressures. Science 311:644–646
Murakami M, Hirose K, Kawamura K, Sata N, Ohishi Y (2004) Post-perovskite phase transition in $MgSiO_3$. Science 304:855–858
Nagai T, Hattori T, Tsuchiya T, Yamanaka T (1998) First observation of $FeGeO_3$-perovskite under high pressure. Solid State Comm 107:223–225
Oganov AR, Ono S (2004) Theoretical and experimental evidence for a post-perovskite phase of $MgSiO_3$ in Earth's *D″* layer. Nature 430:445–448
Oganov AR, Brodholt JP, Price GD (2001) Ab initio elasticity and thermal equation of state of $MgSiO_3$. Earth Planet Sci Lett 184:555–560
Ono S, Kikegawa T, Ohishi Y (2006) Equation of state of $CaIrO_3$-type $MgSiO_3$ up to 144 GPa. Am Mineral 91:475–478
Ozima M, Akimoto S (1983) Flux growth of single crystals of $MgGeO_3$ polymorphs (orthopyroxene, clinopyroxene, and ilmenite) and their phase relations and crystal structures. Am Mineral 68:1199–1205
Perdew JP, Zunger A (1981) Self-interaction correction to density-functional approximations for many-electron systems. Phys Rev B 23:5048–5079
Ross NL, Hazen RM (1990) High-pressure crystal chemistry of $MgSiO_3$ perovskite. Phys Chem Miner 17:228–237
Ross NL, Navrotsky A (1988) Study of the $MgGeO_3$ polymorphs (orthopyroxene, clinopyroxene, and ilmenite structures) by calorimetry, spectroscopy, and phase equilibria. Am Mineral 73:1355–1365
Shen G, Rivers ML, Wang Y, Sutton SR (2001) Laser heated diamond cell system at the Advanced Photon Source for in situ X-ray measurements at high pressure and temperature. Rev Sci Instrum 72:1273–1282
Shieh SR, Duffy TS, Shen G (2004) Elasticity and strength of calcium silicate perovskite at lower mantle pressures. Phys Earth Planet Inter 143–144:93–106
Shieh SR, Duffy TS, Kubo A, Shen G, Prakapenka VB, Sata N, Hirose K, Ohishi Y (2006) Equation of state of the postperovskite phase synthesized from a natural (Mg,Fe)-SiO_3 orthopyroxene. Proc Natl Acad Sci USA 103:3039–3043
Shim S-H, Duffy TS (2000a) Constraints on the *P–V–T* equation of state of $MgSiO_3$ perovskite. Am Mineral 85:354–363
Shim S-H, Duffy TS, Shen G (2000b) The equation of state of $CaSiO_3$ perovskite to 108 GPa at 300 K. Phys Earth Planet Inter 120:327–338

Shim S-H, Duffy TS, Shen G (2001) Stability and structure of $MgSiO_3$ perovskite to 2300-kilometer depth in the Earth's mantle. Science 293:2437–2440

Shim S-H, Duffy TS, Jeanloz R, Shen G (2004) Stability and crystal structure of $MgSiO_3$ perovskite to the core-mantle boundary. Geophys Res Lett 31:L10603

Singh AK (1993) The lattice strains in a specimen (cubic system) compressed nonhydrostatically in an opposed anvil device. J Appl Phys 73:4278–4286

Speziale S, Duffy TS (2002) Single-crystal elastic constants of fluorite (CaF_2) to 9.3 GPa. Phys Chem Miner 29:465–472

Stackhouse S, Brodholt JP, Wookey J, Kendall J-M, Price GD (2005) The effect of temperature on the seismic anisotropy of the perovskite and post-perovskite polymorphs of $MgSiO_3$. Earth Planet Sci Lett 230:1–10

Tsuchiya J, Tsuchyia T, Wentzcovitch RM (2005) Vibrational and thermodynamic properties of $MgSiO_3$ postperovskite. J Geophys Res 110:B02204

Vanpeteghem CB, Zhao J, Angel RJ, Ross NL, Bolfan-Casanova N (2006) Crystal structure and equation of state of $MgSiO_3$ perovskite. Geophys Res Lett 33:L03306

Walter MJ, Kubo A, Yoshino T, Brodholt J, Koga KT, Ohishi Y (2004) Phase relations and equation-of-state of aluminous Mg-silicate perovskite and implications for Earth's lower mantle. Earth Planet Sci Lett 222:501–516

Wang Y, Weidner DJ, Liebermann RC, Zhao Y (1994) *P–V–T* equation of state of $(Mg,Fe)SiO_3$ perovskite: constraints on composition of the lower mantle. Phys Earth Planet Inter 83:13–40

Wentzcovitch RM, Tsuchiya T, Tsuchiya J (2006) $MgSiO_3$ postperovskite at *D″* conditions, Proc Natl Acad Sci USA 103:543–546

Wookey J, Stackhouse S, Kendall J-M, Brodholt J, Price GD (2005) Efficacy of the post-perovskite phase as an explanation for lowermost-mantle seismic properties. Nature 438:1004–1007

Xia X, Weidner DJ, Zhao H (1998) Equation of state of brucite: single crystal Brilluoin spectroscopy study and polycrystalline pressure–volume–temperature measurement. Am Mineral 83:68–74